

## Article

# PDT-Induced Variations of Radachlorin Fluorescence Lifetime in Living Cells In Vitro

Andrey V. Belashov <sup>1</sup>, Anna A. Zhikhoreva <sup>1</sup>, Anna V. Salova <sup>2</sup>, Tatiana N. Belyaeva <sup>2</sup>, Ilia K. Litvinov <sup>2</sup>, Elena S. Kornilova <sup>2</sup> and Irina V. Semenova <sup>1,\*</sup>

<sup>1</sup> Ioffe Institute, Russian Academy of Sciences, 26 Polytekhnicheskaya, St. Petersburg 194021, Russia; belashov.andrey.93@gmail.com (A.V.B.)

<sup>2</sup> Institute of Cytology, Russian Academy of Sciences, 4 Tikhoretsky pr., St. Petersburg 194064, Russia

\* Correspondence: irina.semenova@mail.ioffe.ru

**Abstract:** Variations in the fluorescence lifetimes of Radachlorin photosensitizers in HeLa and A549 cells, caused by photodynamic treatment, were studied using fluorescence lifetime imaging microscopy (FLIM). An analysis of FLIM images of the cells demonstrated a substantial decrease in the mean Radachlorin fluorescence lifetime and intensity as a result of UV irradiation of the photosensitized cells at different doses, with higher doses causing a more pronounced decrease in the mean fluorescence lifetime in cells. The post-treatment decrease in Radachlorin fluorescence intensity was accompanied by the appearance of an additional rapidly decaying fluorescence component and a nonlinear decrease in the weighted fluorescence lifetime obtained from double-exponential fits of time-resolved fluorescence signals. Experiments performed in the aqueous solutions of the photosensitizer revealed similar irreversible changes in the Radachlorin fluorescence lifetime and intensity. Therefore, the observed phenomena occurred most likely due to the photodegradation of the photosensitizer molecules and can be applied for dosimetry and monitoring of irradiation doses in different areas of malignant tissues in the course of photodynamic treatment.

**Keywords:** fluorescence lifetime imaging microscopy; photosensitizer; Radachlorin; photodynamic treatment; photobleaching; time-resolved fluorescence



**Citation:** Belashov, A.V.; Zhikhoreva, A.A.; Salova, A.V.; Belyaeva, T.N.; Litvinov, I.K.; Kornilova, E.S.; Semenova, I.V. PDT-Induced Variations of Radachlorin Fluorescence Lifetime in Living Cells In Vitro. *Photonics* **2023**, *10*, 1262. <https://doi.org/10.3390/photonics10111262>

Received: 29 September 2023

Revised: 23 October 2023

Accepted: 2 November 2023

Published: 15 November 2023



**Copyright:** © 2023 by the authors. Licensee MDPI, Basel, Switzerland. This article is an open access article distributed under the terms and conditions of the Creative Commons Attribution (CC BY) license (<https://creativecommons.org/licenses/by/4.0/>).

## 1. Introduction

Besides the utilization of high-performance photosensitizers with targeted delivery to tumor tissues, the efficient implementation of photodynamic therapy (PDT) requires a sufficient amount of reactive oxygen species (ROS) to be generated in a malignant tumor. This makes reliable PDT dosimetry very important for successful cancer treatment [1–3]. In particular, PDT dosimetry can be based on the estimation of the delivered light dose [4,5] and photosensitizer (PS) concentration in tumor tissues [6,7]; however, an assessment of the resulting dose requires the application of a special model providing a combination of these data [3,8]. This approach for the estimation of effectively generated ROS is unlikely to be very accurate due to a variety of processes affecting light penetration through tissues [9], different levels of tissue oxygenation [10], and the intracellular distribution of a particular photosensitizer [11,12]. The estimation of the PDT dose via the detection of singlet oxygen phosphorescence is very difficult [13,14], yet possible in clinical practice, although it is informative for the estimation of photosensitizer efficacy in experiments in model solutions [15,16] and in living cells in vitro [17,18]. Another common approach that can be used for real-time PDT dosimetry relies on the monitoring of photosensitizer fluorescence intensity [19–21]. However, the accuracy of this approach is quite low due to the non-uniformity of the absorption and scattering properties of tissues [22,23], as well as the potential dependence of fluorophore fluorescence intensity on microenvironment properties, acidity in particular [24]. Nevertheless, an analysis of the distributions of

photosensitizer fluorescence intensity is applied for the intraoperative delimitation of tumor boundaries [25,26].

An analysis of the photobleaching kinetics of a PS can also be used for evaluation of the PDT dose, so far as ROS tend to cause the destruction of both the intracellular compartments and the PS molecules themselves [27–29]. However, being also based on the detection of fluorescence intensity, which depends not only on the amount of fluorescent molecules but also on their fluorescence quantum yield, diffusion, absorption, and scattering in tissues, this approach suffers from low accuracy. The autofluorescence of tissues and potential fluorescence signals from photoproducts produced in the course of PS bleaching [27,30] may also contribute to the resulting signal and produce erroneous data. Meanwhile, time-resolved fluorescence lifetime measurements basically do not depend on the fluorophore concentration, the intensity of excitation light, and scattering and absorption properties of the surrounding tissues. The fluorescence lifetime can be sensitive to many parameters of the surrounding microenvironment, including acidity, temperature, viscosity, and the presence of specific quenchers [31–33], which makes this parameter quite informative in the analysis of PS behavior during photodynamic treatment of cells and tissues. A multi-exponential analysis of the obtained time-resolved data allows for the robust separation of signals from different fluorescent species [34] and for sorting the autofluorescence signal [35]. The analysis of time-resolved fluorescence signals was applied for characterization of various PSs in solutions [36], cells in vitro [37,38], and tissues in vivo [39,40]. The utilization of fluorescence lifetime spectroscopy and microscopy allowed for the analysis of photoproduct formation [41,42], the intracellular localization of PS molecules [24,38], and their internalization in an aggregated form [43].

We have recently shown that time-resolved fluorescence spectroscopy using Radachlorin allows assessing variations in microenvironmental acidity, polarity, and viscosity [24,36,44]. The FLIM-assisted imaging provided data on the PS uptake, concentration, and fluorescence quantum yield in cells and tissues [24]. In this study, we present an analysis of changes in the fluorescence characteristics of Radachlorin in cells in vitro as a result of photodynamic treatment.

## 2. Materials and Methods

### 2.1. Radachlorin Photosensitizer

The experiments were performed with Radachlorin (RadaPharma, Russia), a second-generation clinically approved PS comprising a composition of sodium salts of chlorin e6 (~80%), purpurin 5 (~15%), and chlorin p6 (~5%). Molecular structures of Radachlorin constituents are depicted in Figure 1a. Molecular weights of the constituents comprised: chlorin e6—596.7 g/mol, chlorin p6—582.6 g/mol, and purpurin 5—566.6 g/mol. Radachlorin is produced in different formulations: a water-soluble concentrate for preparation of solutions for intravenous infusion, a solution for treatment of various medical conditions in the oral cavity, and gels for treatment of skin diseases [45]. The stock solution for intravenous injections, which is easily dissolved in water and water–alcohol solutions, cell culture media, etc., was used in the experiments.

Radachlorin has been applied in clinical practice for a relatively long time, so its performance in patients in vivo is predictable with sufficient reliability. The PS was shown to be efficient in PDT of various malignancies: non-melanoma skin cancers [46,47], early esophageal cancer [48], non-small-cell lung cancer [49], cholangiocarcinoma [50], and some other cancers. The drug is also applied for treatment of some benign conditions and is used as an antibacterial [51] and antiviral [52] agent.

Different aspects of variations in the photophysical properties of Radachlorin with microenvironment pH, polarity, and viscosity were intensively studied in solutions. These properties included absorption and fluorescence spectra, fluorescence quantum yield and lifetimes, fluorescence anisotropy, and rotational diffusion time (see [44] and references therein) as well as quantum yield and characteristic times of singlet oxygen

phosphorescence [16]. However, some subtle processes of its performance on the cellular level are still unknown.

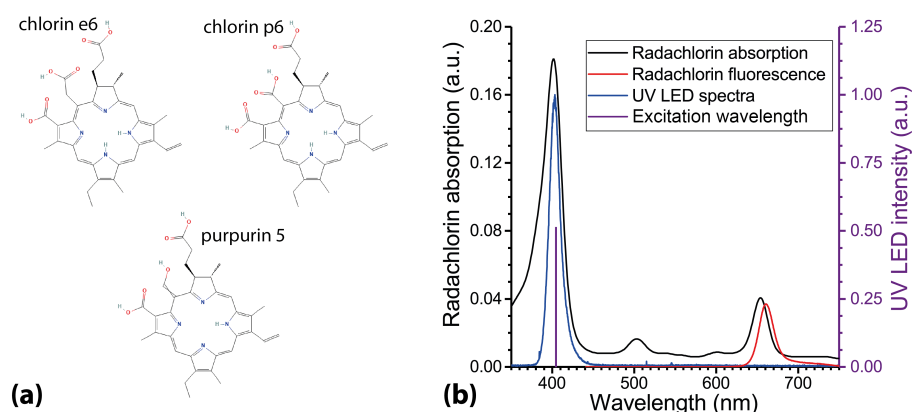


**Figure 1.** (a) Molecular structures of Radachlorin components. (b) Radachlorin absorption and emission spectra and emission spectrum of the UV LED light source utilized for photodynamic treatment of living cells. Radachlorin emission spectrum was obtained in aqueous solution at pH 7.5, with Radachlorin concentration of 20  $\mu\text{g}/\text{mL}$  and laser excitation at 405 nm.

## 2.2. Cell Cultures

Fluorescence lifetime imaging of Radachlorin PS in living cells was performed on cell samples of two established lines: human cervix epidermoid carcinoma HeLa and human alveolar basal epithelial adenocarcinoma A549. Cell lines were obtained from the Institute of Cytology, the shared research facility “Vertebrate cell culture collection”, supported by the Ministry of Science and Higher Education of the Russian Federation (Agreement #075–15-2021–683). Cells were cultivated in the Dulbecco’s modified eagle medium (DMEM) supplemented with 10% fetal bovine serum and 1% penicillin–streptomycin at 37 °C in 5%  $\text{CO}_2$  atmosphere during 48 h. Then, Radachlorin was added to the culture medium at the concentration of 20  $\mu\text{g}/\text{mL}$  (33.5  $\mu\text{M}$ ), and cells were cultivated further for 24 h in dark conditions to prevent the unintentional photodynamic treatment and PS photobleaching. No dark toxicity of Radachlorin was observed in control experiments when analyzing the survival of HeLa and A549 cells incubated in Radachlorin solutions with PS concentrations of 10, 20, and 40  $\mu\text{g}/\text{mL}$ . No ethidium bromide or annexin-V fluorescence featuring cell necrosis and apoptosis, respectively, were detected after 48-hour incubation of photosensitized cells in dark conditions.

## 2.3. FLIM of Intracellular Radachlorin

Recording of FLIM data was performed using the TCSPC technique with a confocal fluorescence scanning module DCS-120 from Becker & Hickl installed on a Nikon T12-A inverted fluorescence microscope. Recording of fluorescence images was performed at excitation of PS molecules with a 405 nm picosecond laser BDS-SM-405-PS-101 operating at a repetition rate of 20 MHz and a power density of 0.15  $\text{mW}/\text{cm}^2$ . Time-resolved signals of Radachlorin fluorescence were recorded in a single-photon counting mode using a hybrid GaAsP photodetector HPM-100-40 (Becker & Hickl, Berlin, Germany) with an instrumental response time accuracy of 120 ps. Spectral selection of Radachlorin fluorescence from weak autofluorescence of living cells was provided via a bandpass optical filter with a transmission band of 608–683 nm. Physiologic conditions of live cell samples (37 °C, 5%  $\text{CO}_2$  atmosphere) in the course of monitoring were provided via a H301-mini incubator (Okolab, Japan) installed in the microscope. A 60 $\times$ , NA = 1.49 microscope lens (Nikon, Japan) was used for FLIM monitoring of living cells with a 90  $\times$  90  $\mu\text{m}$  field of view. The collection of fluorescence signals from cell samples for 50 s at relatively low irradiation power density allowed for avoiding significant impact on living cells. The pixelwise fitting of the obtained time-resolved signals was performed with SPCImage software 8.5 NG (Becker & Hickl, Germany), which included convolution of a decay function with

the automatically approximated IRF. A preliminary  $3 \times 3$  pixel binning of FLIM data allowed us to obtain robust time-resolved signals typically with 8000–12,000 photons (when monitoring cells before PDT).

The control experiments showed that saturation of the accumulated photosensitizer in cells was attained after 4–6 h of cell incubation in the Radachlorin solution in DMEM. No statistically significant changes in the mean Radachlorin fluorescence lifetime were observed in cells incubated with Radachlorin for 4, 6, 8, or 24 h. The potential undesired photobleaching of intracellular Radachlorin during incubation was avoided by keeping cell samples in dark conditions. Therefore, variations in the fluorescence lifetime observed after excitation could be attributed to the effect of cell irradiation and the generation of reactive oxygen species. It should be mentioned that, in general, some variability in the mean Radachlorin fluorescence lifetime was observed among individual cells. Typical variations of this parameter in HeLa and A549 cells amounted to  $\pm 0.3$  ns and  $\pm 0.4$  ns, respectively. The diversity of the mean lifetime of Radachlorin fluorescence could be due to slightly different amounts of the photosensitizer accumulated in the lysosomes and cytoplasm of the cells at different stages of the cell cycle and different pH levels of intracellular media in them, since the acidity of the surrounding microenvironment can significantly affect Radachlorin fluorescence lifetime [24]. Despite the diversity of the mean fluorescence lifetime among individual cells, the applied experimental protocol of consecutive monitoring and analysis of the same set of microscopic fields of view allowed robust distinguishing of variations in the fluorescence properties of the intracellular photosensitizer.

#### 2.4. Photodynamic Treatment of Cells and Analysis of Their Response

Photodynamic treatment of living cells was performed using a UV LED light source with the emission spectrum roughly coinciding with the Soret absorption band of Radachlorin, as shown in Figure 1b. Two sets of experiments were performed, allowing for varying the PDT dose by changing either the irradiation power density or duration. In the first set, the irradiation power density was varied in the range of 13–46 mW/cm<sup>2</sup> by installing a proper set of optical filters, while the irradiation duration remained the same and equaled 5 min. In another set of experiments, the irradiation time was varied from 140 to 460 s at a constant power density of UV LED of 27 mW/cm<sup>2</sup>. In both cases, the irradiation dose was varied within approximately the same range, from 3.8 to 12.4 J/cm<sup>2</sup>. Note that utilization of the broadband UV LED rather than a 405-nm laser allowed us to achieve homogeneous irradiation of the entire sample and to avoid speckle noise.

The choice of specific irradiation doses was based on the results of our previous works [53,54], where treatment conditions, typically leading to the apoptotic and necrotic pathways of cell death for cells of various types, were determined. Cell death via necrosis was confirmed using the acridine orange and ethidium bromide test assay, while apoptosis was detected using an Annexin-V fluorescence stain. Observation of changes in cellular morphology after photodynamic treatment was performed using the differential interference contrast (DIC) microscopy on a Nikon TI2-A inverted fluorescence microscope.

#### 2.5. Radachlorin Photobleaching in Aqueous Solution

The dynamics of Radachlorin photobleaching in cells were compared with those in aqueous solutions. In these experiments, a Petri dish containing 200  $\mu$ L of PS solution in water at the concentration of 5  $\mu$ L/mL was installed in the FLIM microscope and continuously irradiated via the same UV LED source at the power density of 55 mW/cm<sup>2</sup>. Due to the relatively thin layer of PS solution in the Petri dish of about 0.2 mm thick and the low PS concentration, the absorption of exciting radiation did not exceed 15%, allowing us to achieve high uniformity of the photobleaching speed in the entire volume of the solution and to avoid an influence of diffusion.

### 3. Results and Discussion

#### 3.1. Dose-Dependent Changes in Cellular Morphology in Response to Photodynamic Treatment

The response of living cells to photodynamic treatment with Radachlorin was analyzed at several irradiation doses, ranging from 3.8 to 12.4 J/cm<sup>2</sup>. The sets of DIC microscopy images and fluorescence lifetime images of the same fields of view in the cell samples were obtained. It was shown that at low doses the typical cellular response included cell shrinkage and rounding, and formation of small blebs on cellular membranes, featuring the apoptotic pathway of cell death (see sets of DIC images corresponding to the irradiation power densities from 13 to 31 mW/cm<sup>2</sup> in Figure 2). Higher irradiation doses yielded another pattern of changes in the cell morphology, including formation of big blebs and minor increases in the contrast of intracellular structures, indicating membrane rupture and ongoing cell necrosis (see sets of DIC images corresponding to the power densities of 40 and 46 mW/cm<sup>2</sup> in Figures 2 and 3, respectively). It is worth noting that despite the sufficiently homogeneous distribution of UV light among the cells, it was hardly possible to induce identical responses from all cells within the field of view. This was due to both the diverse antioxidant activity of cells at different stages of the cell cycle [55,56] and differences in PS accumulation by individual cells, which might vary from one cell to another by more than 30%, as we have shown in [54].

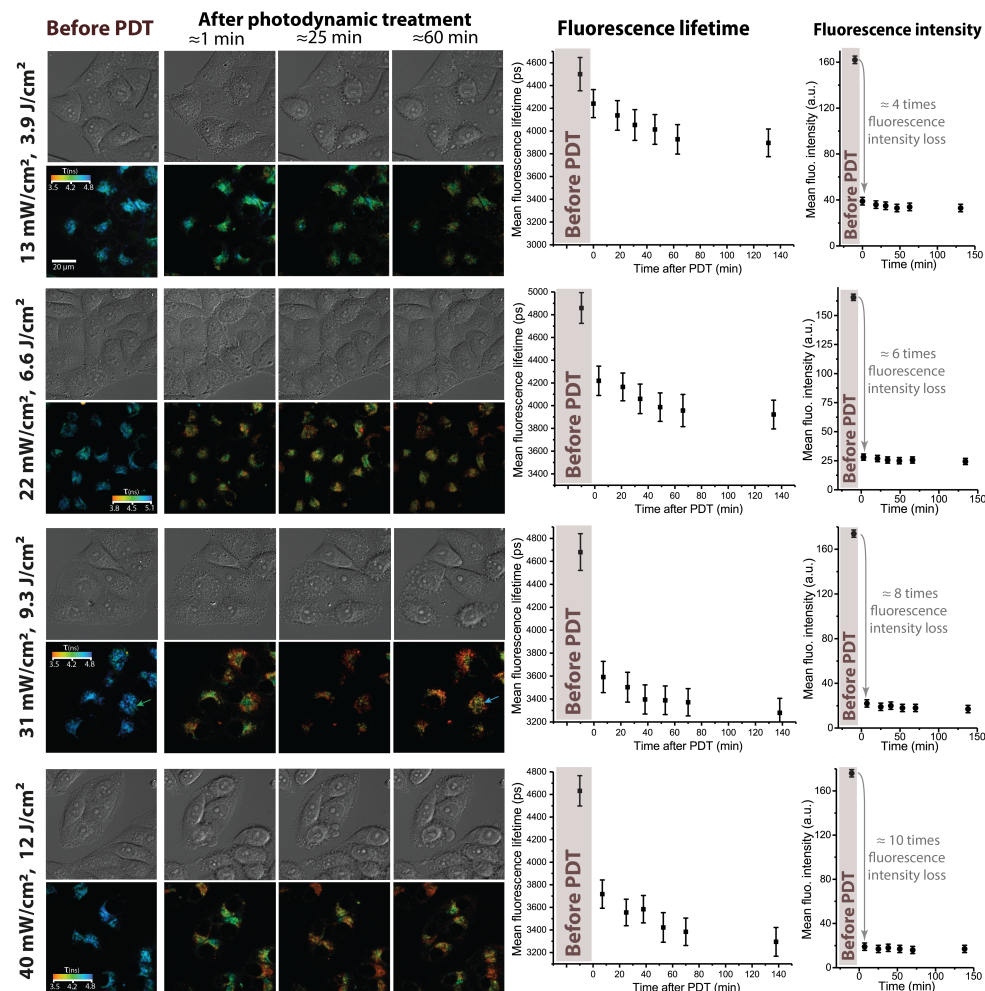


**Figure 2.** Response of HeLa cells to photodynamic treatment with Radachlorin at different irradiation doses varied by changing the UV LED power density. The power density and corresponding dose are indicated next to each set of images, the irradiation duration comprised 5 min. Images on the (left): DIC microscope images and corresponding FLIM images of Radachlorin fluorescence. On the (right): mean Radachlorin fluorescence lifetime and intensity as a function of time before and after irradiation.

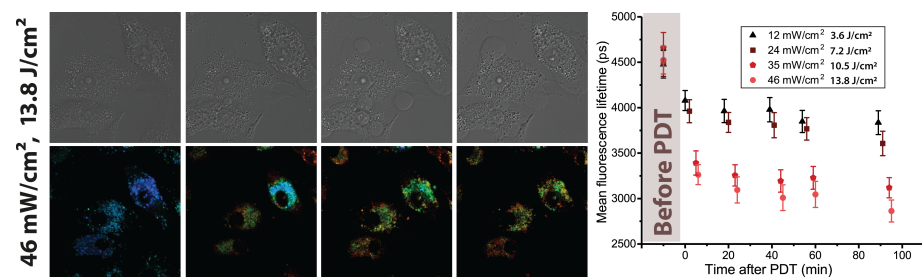


**Figure 3.** Response of A549 cells to UV LED irradiation. On the (left): DIC microscope images and Radachlorin fluorescence lifetime images before and after 5 min irradiation at  $46 \text{ mW/cm}^2$ . On the (right): mean Radachlorin fluorescence lifetime as a function of time after 5-min irradiation of cells at different power densities.

### 3.2. Fluorescence Lifetimes of Radachlorin in Living Cells before and after Photodynamic Treatment

The analysis of time-resolved Radachlorin fluorescence signals and their further pixel-wise fitting with a single-exponential function allowed us to observe the noticeable decrease in the PS fluorescence lifetime  $\tau_{fl}$  following sample irradiation. Four sets of the FLIM images of Radachlorin shown in Figure 2 clearly demonstrate the decrease in color-encoded fluorescence lifetime by 10–25%, depending on the irradiation power density applied to the sample. Moreover, the initial rapid drop in the Radachlorin fluorescence lifetime gradually rose with the irradiation dose (see plots of the mean fluorescence lifetime in Figure 2). Similar patterns were observed in A549 cells, where the typical Radachlorin fluorescence lifetimes were slightly lower than those in HeLa cells (see Figure 3) and the increase in the irradiation power density led to a more significant decrease in  $\tau_{fl}$ .

As can be seen from the plots in Figure 2, the most prominent decrease in Radachlorin fluorescence lifetime occurred between the measurements corresponding to cells before and right after irradiation, and this drop became more pronounced with the increasing dose. A somewhat slower, although noticeable, decrease in the mean fluorescence lifetime of the order of 0.3–0.4 ns was observed further for several dozens of minutes after irradiation. This prolonged decrease in the Radachlorin fluorescence lifetime could not be due to cell monitoring via FLIM since the typical dose of UV irradiation in the course of monitoring did not exceed  $7.5 \text{ mJ/cm}^2$ , which is several hundred times lower than the doses used for photodynamic treatment. Moreover, corresponding variations in the average fluorescence intensity (right column in Figure 2) demonstrated that almost no photobleaching of the photosensitizer occurred after the photodynamic treatment. The observed minor variations in the fluorescence intensity were within measurement error bars, limited by variations in the cell morphology and Z-drift of the microscope stage.

The statistical analysis of FLIM images of cells obtained at the same irradiation dose but demonstrating different morphological changes has shown that the decrease in mean fluorescence lifetime depended solely on the irradiation dose and did not depend on the individual cellular response. As can be seen from each set of FLIM images in Figure 2, irrespective of changes in cell morphology within the field of view, the Radachlorin fluorescence lifetime varied by a similar amount in all the cells. This evidences that the decrease in fluorescence lifetime did not occur due to specific processes involved in apoptosis or necrosis but rather resulted from basic chemical and photochemical processes in cells triggered by photodynamic treatment. The noticeable decrease in Radachlorin fluorescence lifetime was evident even in cells that did not show any changes in morphology in response to treatment.

Similar variations in the PDT dose were also performed by changing the irradiation time in the range from 140 to 460 s at the constant power density of  $27 \text{ mW/cm}^2$ . This provided variations in the PDT dose in a range of  $3.8\text{--}12.4 \text{ J/cm}^2$ . The sets of obtained FLIM and DIC images and the dynamics of the Radachlorin fluorescence lifetime in HeLa cells are shown in Figure 4. The comparison of data in Figures 2 and 4 shows that Radachlorin fluorescence lifetime exhibited similar behavior as a function of irradiation dose, regard-

less of whether it was varied by changing the irradiation duration or power density. As can be seen from the graphs in Figures 2 and 4, the initial rapid decrease in Radachlorin fluorescence lifetime in the course of irradiation was followed by its further minor and slow decrease. The increase in irradiation dose resulted in a more significant initial drop in the mean Radachlorin fluorescence lifetime in the treated cells. However, although the two applied scenarios of dose variations provided about the same doses at each step, the extent of the decrease in mean fluorescence lifetime was somewhat different. Therefore, not only the dose itself but also the regime of its delivery affected the extent of the decrease in Radachlorin fluorescence lifetime. This result correlates well with our previous findings, which showed that variations in the PDT mode resulted in different cell responses, observed using digital holographic microscopy [57]. Since one of the main factors causing Radachlorin photobleaching is interactions with ROS, the observed tendencies can be due to their different rates of generation in cells and are indicative that not only the amount of generated ROS determines both cell responses and dynamics of Radachlorin fluorescence lifetime but also the generation rate is influential as well. Notably, some shortening of the fluorescence lifetime after irradiation was also observed in another porphyrin derivative, Talaporfin sodium, in W31 and WFB cells [58].

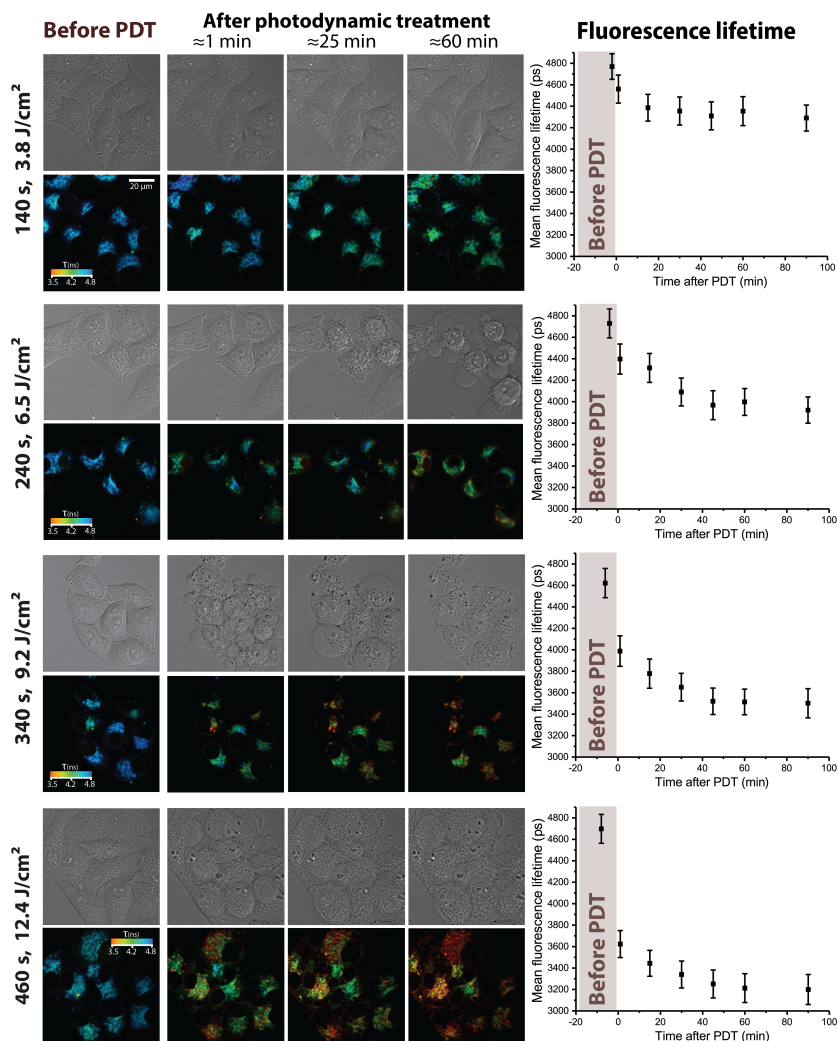


**Figure 4.** Response of HeLa cells to photodynamic treatment with Radachlorin at different irradiation doses varied by changing the irradiation duration. The irradiation duration and corresponding dose are indicated next to each set of images, the irradiation power density comprised  $27 \text{ mW/cm}^2$ . Images on the (left): DIC microscope images and corresponding FLIM images of Radachlorin fluorescence. On the (right): mean Radachlorin fluorescence lifetime as a function of time before and after irradiation.

### 3.3. Radachlorin Photobleaching in Aqueous Solution

The observed variations in Radachlorin fluorescence lifetime after photodynamic treatment could result either from changes in the microenvironment (in particular, we have recently observed the strong dependence of Radachlorin fluorescence lifetime on the pH and polarity of the surrounding medium [24]) or from photoinduced modifications of the Radachlorin molecules themselves. The potential variations in the microenvironment properties were not induced via specific intracellular biochemical reactions accompanied by either apoptotic or necrotic cell death, as the actual decrease in Radachlorin fluorescence lifetime occurred at the very first minutes of irradiation, and a similar decrease in lifetime was observed in all individual cells independently based on their specific response to treatment. Therefore, we believe that photosensitizer photobleaching was mostly responsible for the observed phenomena. To validate this assumption, we performed a set of experiments aimed at the analysis of Radachlorin photobleaching dynamics in an aqueous solution by monitoring its fluorescence intensity and decay traces during continuous irradiation of the solution.

The results obtained for the variations in the fluorescence lifetimes and intensity in the course of photobleaching are shown in Figure 5a. As can be seen from Figure 5a, the decrease in Radachlorin fluorescence intensity of more than two orders of magnitude was observed within 20 min of solution irradiation by the UV LED at the power density of  $55 \text{ mW/cm}^2$ . The kinetics of fluorescence intensity (black curve) is followed by the decrease in the fluorescence lifetime (blue dots), which is accompanied by the appearance of a rapidly decaying component (see time-resolved fluorescence signals in Figure 5b). When fitted with a single-exponential function, the time-resolved signals provided fluorescence lifetime values, which decreased from 3.4 ns to 2.4 ns (see filled blue circles in Figure 5a). A more accurate double-exponential fitting of the fluorescence decay traces showed a gradual increase in the portion of a rapidly decaying component with a lifetime of  $1.0 \pm 0.4 \text{ ns}$  up to 65% and a decrease down to 35% of the portion of a component with a longer lifetime of  $3.8 \pm 0.4 \text{ ns}$ . Note that the indicated fluorescence lifetimes of the two components are mean values obtained from several experiments. The mean weighted fluorescence lifetime is plotted in Figure 5a by empty light-blue rhombi. As can be seen from the plot, the dynamics of the mean weighted fluorescence lifetime coincides well with the kinetics of fluorescence intensity.

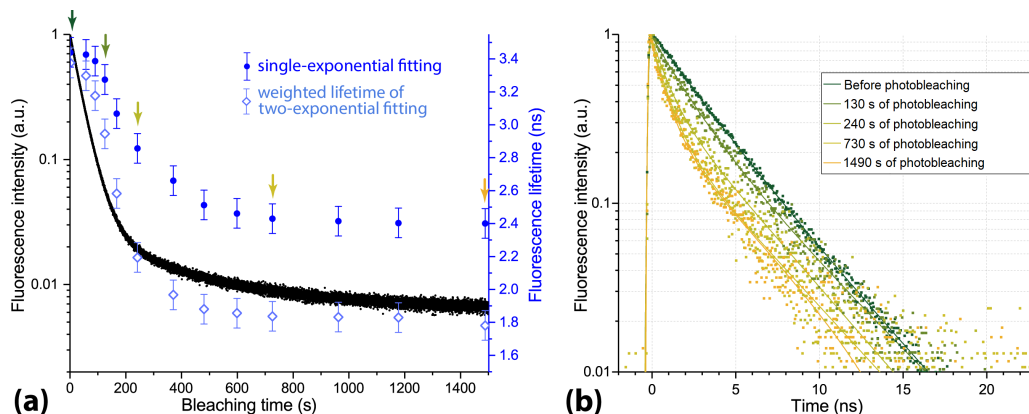


**Figure 5.** (a) Fluorescence intensity and lifetime of aqueous solution of Radachlorin under continuous irradiation by UV LED at the power density of  $55 \text{ mW/cm}^2$ . The fluorescence lifetime obtained from the single-exponential fitting is shown with blue-filled circles, and the mean weighted fluorescence lifetime obtained from the double-exponential fitting is shown with light-blue rhombi. (b) Time-resolved fluorescence signals obtained at different stages of the photobleaching process. Color arrows in (a) indicate the actual time when the corresponding time-resolved signals in (b) were recorded.

The observed conformity of the dynamics of Radachlorin fluorescence lifetime in aqueous solution and in cells suggests that photobleaching of the photosensitizer was

mainly due to light-induced transformations of its molecules rather than to interactions with specific intracellular microenvironments. Another set of control experiments confirmed that the decrease in fluorescence lifetimes caused by photobleaching was irreversible, and Radachlorin fluorescence did not recover for at least 6 h after the irradiation. Note that the similar behavior of the fluorescence lifetime as a result of photobleaching has been reported for some other fluorophores [59–63]. Variations in the fluorescence lifetime observed in our experiments can be explained by the formation of free radicals enhancing fluorescence quenching and accelerating the depletion of the excited states of photosensitizer molecules through nonradiative transitions, resulting in the decrease in the fluorescence lifetime.

A relatively low amount of photons available for registration in live-cell experiments (especially when working with the partially photobleached photosensitizer) does not allow for an accurate investigation of whether a single- or double-exponential fitting model is more suitable for a particular application. Another factor affecting the choice of a fitting model is the diversity of microenvironment properties (pH, polarity, viscosity, etc.) in the intracellular compartments, which may cause variations in the fluorescence lifetimes. Therefore, in contrast with the experiments on Radachlorin photobleaching in aqueous solutions, where the appearance of the rapidly decaying fluorescence component was clearly visible, a robust conclusion on a similar effect in living cells after their irradiation is hardly possible. However, an analysis of the chi-squared parameter has shown a slight increase in its value after the photodynamic treatment of cells. The typical mean chi-square of the single-exponential fits of Radachlorin fluorescence signals in non-irradiated cells laid within the range of 1.04 to 1.13, while cell irradiation led to an increase in this parameter up to the range of 1.2 to 1.36. Two examples of the time-resolved signals fitted with single-exponential function along with the residual plots corresponding to the control cells and cells exposed to treatment are shown in Figure 6. As can be seen from Figure 6, the irradiation of photosensitized cells by UV LED resulted in a more rapid decay of fluorescence signals. Moreover, similar to that in aqueous solution (Figure 5), the fluorescence decay kinetics in cells after their irradiation was fitted more accurately by a double-exponential function with the appearance of the second, more rapidly decaying component (see Figure 6b).

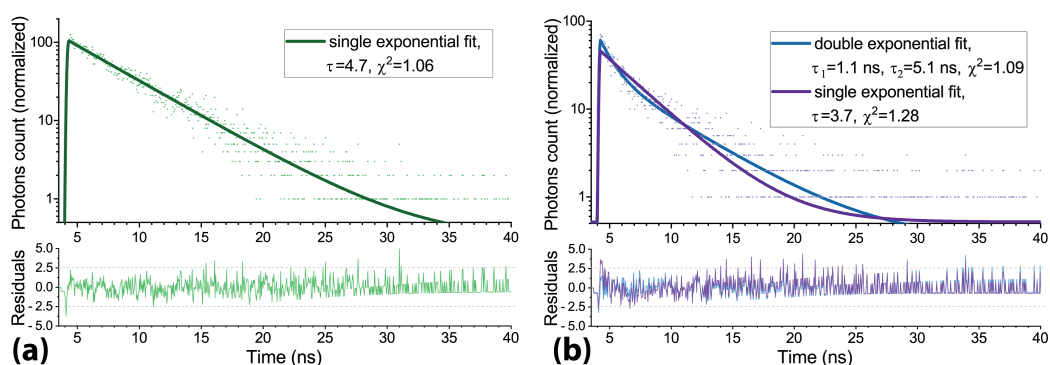


**Figure 6.** (a) Radachlorin fluorescence decay trace in HeLa cells before irradiation and its single-exponential fit. (b) Radachlorin fluorescence decay trace in HeLa cells after irradiation and its single- and double-exponential fits.

Definitely, the conditions of PS photobleaching in cells are quite different from those in solutions. The differences are both in the physical characteristics (polarity, pH, and viscosity) and the chemical composition of the surrounding medium, including the presence of various organic substances, antioxidants, and quenchers of singlet oxygen and other ROS. Moreover, the intracellular distribution of the three Radachlorin components may also differ, although the major areas of fluorescence localization are lysosomes [24]. Nevertheless, the observed similarity of Radachlorin photobleaching processes in solutions and cells allows us to consider the analysis of Radachlorin fluorescence lifetime as a promising auxiliary tool for monitoring the effect of photodynamic treatment on cells and tissues.

#### 4. Summary and Conclusions

In this work, we studied variations in the fluorescence lifetimes of Radachlorin photosensitizer in HeLa and A549 cells treated with different doses of UV irradiation, inducing the photosensitized generation of reactive oxygen species. Cells irradiation at different doses resulted in diverse changes in their morphology, as recorded using DIC microscopy. The analysis of FLIM images of PS-containing cells demonstrated the substantial decrease in the mean Radachlorin fluorescence lifetime and intensity after cell irradiation at all the applied doses. Experiments performed in aqueous solutions revealed similar irreversible changes in Radachlorin fluorescence lifetime and intensity as a result of photobleaching. The decrease in Radachlorin fluorescence intensity during photobleaching was accompanied by the appearance of the rapidly decaying fluorescence component and the nonlinear decrease in both single-exponential fluorescence lifetime and weighted double-exponential fluorescence lifetime. The extent of the decrease in Radachlorin fluorescence lifetime as a result of photodynamic treatment of HeLa and A549 cells was related to the irradiation dose: the dose increase (by either increase of irradiation duration or power density) caused a more significant decrease in the mean fluorescence lifetime inside the cells. However, the two regimes of dose variation led to slightly different extents of the decrease in mean fluorescence lifetime. The observed phenomena was likely to occur due to photodegradation of the PS molecules, in particular, because of the production of PS quenchers, specifically ROS, during PDT, as well as due to different fluorescence lifetimes and photostability of Radachlorin constituents.

The observed tendencies of the decrease in Radachlorin fluorescence lifetime due to PDT can be used for PDT dosimetry and monitoring of irradiation doses in different areas of malignant tissues. The more common method of PDT dosimetry based on the analysis of slow losses in fluorescence intensity during photobleaching [64–66] has some disadvantages over monitoring the decrease in the fluorescence lifetime reported in this study. The major disadvantage is the dependence of the detected fluorescence intensity on excitation and emission light scattering, the impact of fluorescence quantum yield, and the diffusion of PS molecules. The fluorescence lifetime affected by PS photobleaching can be used as a more robust and independent indicator of Radachlorin photodegradation. We believe that further development of this approach based on the observed changes in the fluorescence lifetime during PDT may lead to novel methods for the assessment of PDT efficacy.

**Author Contributions:** Conceptualization, A.V.B. and I.V.S.; methodology, A.V.B., A.V.S. and I.V.S.; cell cultivation and control experiments, T.N.B., I.K.L. and E.S.K.; investigation, A.V.B. and A.A.Z.; validation, A.A.Z. and A.V.S.; writing, A.V.B., A.A.Z. and I.V.S. All authors have read and agreed to the published version of the manuscript.

**Funding:** A.V.B., A.A.Z., A.V.S. and I.V.S. acknowledge the financial support from the Russian Science Foundation (grant: #21-72-10044). T.N.B., I.K.L. and E.S.K. acknowledge the financial support from the Ministry of Science and Higher Education of the Russian Federation (state contract: # 2021-0005).

**Institutional Review Board Statement:** Not applicable.

**Data Availability Statement:** Data are available within the paper.

**Acknowledgments:** The experiments on intracellular Radachlorin fluorescence lifetimes before and after PDT under different irradiation doses, FLIM data collection and processing, the investigation of Radachlorin photobleaching in aqueous solution, and the analysis of time-resolved signals were carried out by A.A.Z., A.V.B., A.V.S. and I.V.S. in the framework of the RSF project (#21-72-10044). Cell cultivation and control experiments on Radachlorin dark phototoxicity were performed by T.N.B., I.K.L. and E.S.K. under financial support from the Ministry of Science and Higher Education of the Russian Federation.

**Conflicts of Interest:** The authors declare no conflict of interest.

## References

1. Jacques, S.L. How tissue optics affect dosimetry of photodynamic therapy. *J. Biomed. Opt.* **2010**, *15*, 051608. [[CrossRef](#)] [[PubMed](#)]
2. Pogue, B.W.; Elliott, J.T.; Kanick, S.C.; Davis, S.C.; Samkoe, K.S.; Maytin, E.V.; Pereira, S.P.; Hasan, T. Revisiting photodynamic therapy dosimetry: Reductionist & surrogate approaches to facilitate clinical success. *Phys. Med. Biol.* **2016**, *61*, R57–R89. [[PubMed](#)]
3. Wilson, B.C.; Patterson, M.S.; Lilge, L. Implicit and explicit dosimetry in photodynamic therapy: A new paradigm. *Lasers Med. Sci.* **1997**, *12*, 182–199. [[CrossRef](#)] [[PubMed](#)]
4. Wilson, B.; Muller, P.; Yanch, J. Instrumentation and light dosimetry for intra-operative photodynamic therapy (PDT) of malignant brain tumours. *Phys. Med. Biol.* **1986**, *31*, 125. [[CrossRef](#)]
5. Profio, A.E.; Doiron, D.R. Dose measurements in photodynamic therapy of cancer. *Lasers Surg. Med.* **1987**, *7*, 1–5. [[CrossRef](#)] [[PubMed](#)]
6. Lilge, L.; O'Carroll, C.; Wilson, B.C. A solubilization technique for photosensitizer quantification in ex vivo tissue samples. *J. Photochem. Photobiol. B Biol.* **1997**, *39*, 229–235. [[CrossRef](#)]
7. Lee, C.C.; Pouge, B.W.; Strawbridge, R.R.; Moodie, K.L.; Bartholomew, L.R.; Burke, G.C.; Jack Hoopes, P. Comparison of Photosensitizer (AlPcS2) Quantification Techniques: In Situ Fluorescence Microsampling Versus Tissue Chemical Extraction. *Photochem. Photobiol.* **2001**, *74*, 453–460. [[CrossRef](#)]
8. Yeh, S.C.A.; Patterson, M.S.; Hayward, J.E.; Fang, Q. Time-resolved fluorescence in photodynamic therapy. *Photonics* **2014**, *1*, 530–564. [[CrossRef](#)]
9. Sandell, J.L.; Zhu, T.C. A review of in vivo optical properties of human tissues and its impact on PDT. *J. Biophotonics* **2011**, *4*, 773–787. [[CrossRef](#)]
10. Georgakoudi, I.; Foster, T.H. Singlet oxygen-versus nonsinglet oxygen-mediated mechanisms of sensitizer photobleaching and their effects on photodynamic dosimetry. *Photochem. Photobiol.* **1998**, *67*, 612–625.
11. Mojzisova, H.; Bonneau, S.; Vever-Bizet, C.; Brault, D. Cellular uptake and subcellular distribution of chlorin e6 as functions of pH and interactions with membranes and lipoproteins. *Biochim. Biophys. Acta (BBA)-Biomembr.* **2007**, *1768*, 2748–2756. [[CrossRef](#)] [[PubMed](#)]
12. Gupta, S.; Dwarakanath, B.; Muralidhar, K.; Jain, V. Cellular uptake, localization and photodynamic effects of haematoporphyrin derivative in human glioma and squamous carcinoma cell lines. *J. Photochem. Photobiol. B Biol.* **2003**, *69*, 107–120. [[CrossRef](#)]
13. Niedre, M.; Patterson, M.S.; Wilson, B.C. Direct Near-infrared Luminescence Detection of Singlet Oxygen Generated by Photodynamic Therapy in Cells In Vitro and Tissues In Vivo. *Photochem. Photobiol.* **2002**, *75*, 382–391. [[CrossRef](#)] [[PubMed](#)]
14. Jarvi, M.T.; Niedre, M.J.; Patterson, M.S.; Wilson, B.C. Singlet oxygen luminescence dosimetry (SOLD) for photodynamic therapy: Current status, challenges and future prospects. *Photochem. Photobiol.* **2006**, *82*, 1198–1210. [[CrossRef](#)] [[PubMed](#)]
15. Nishimura, T.; Hara, K.; Honda, N.; Okazaki, S.; Hazama, H.; Awazu, K. Determination and analysis of singlet oxygen quantum yields of talaporfin sodium, protoporphyrin IX, and lipidated protoporphyrin IX using near-infrared luminescence spectroscopy. *Lasers Med. Sci.* **2020**, *35*, 1289–1297. [[CrossRef](#)]
16. Zhikhoreva, A.A.; Belashov, A.V.; Ignatov, E.S.; Gelfond, M.L.; Semenova, I.V.; Vasyutinskii, O.S. Singlet oxygen generation in aerosol jet and on biological surfaces. *J. Photochem. Photobiol. Biol.* **2022**, *228*, 112395. [[CrossRef](#)]
17. Hatz, S.; Poulsen, L.; Ogilby, P.R. Time-resolved singlet oxygen phosphorescence measurements from photosensitized experiments in single cells: Effects of oxygen diffusion and oxygen concentration. *Photochem. Photobiol.* **2008**, *84*, 1284–1290. [[CrossRef](#)]
18. Morozov, P.; Lukina, M.; Shirmanova, M.; Divochiy, A.; Dudenkova, V.; Gol'tsman, G.N.; Becker, W.; Shcheslavskiy, V.I. Singlet oxygen phosphorescence imaging by superconducting single-photon detector and time-correlated single-photon counting. *Opt. Lett.* **2021**, *46*, 1217–1220. [[CrossRef](#)]
19. Zhu, T.C.; Ong, Y.; Kim, M.M.; Liang, X.; Finlay, J.C.; Dimofte, A.; Simone, C.B., 2nd.; Friedberg, J.S.; Busch, T.M.; Glatstein, E.; et al. Evaluation of light fluence distribution using an IR navigation system for HPPH-mediated pleural photodynamic therapy (pPDT). *Photochem. Photobiol.* **2020**, *96*, 310–319. [[CrossRef](#)]
20. Diamond, K.R.; Malysz, P.P.; Hayward, J.E.; Patterson, M.S. Quantification of fluorophore concentration in vivo using two simple fluorescence-based measurement techniques. *J. Biomed. Opt.* **2005**, *10*, 024007–024007. [[CrossRef](#)]
21. Diamond, K.R.; Patterson, M.S.; Farrell, T.J. Quantification of fluorophore concentration in tissue-simulating media by fluorescence measurements with a single optical fiber. *Appl. Opt.* **2003**, *42*, 2436–2442. [[CrossRef](#)] [[PubMed](#)]
22. Ong, Y.H.; Kim, M.M.; Finlay, J.C.; Dimofte, A.; Singhal, S.; Glatstein, E.; Cengel, K.A.; Zhu, T.C. PDT dose dosimetry for Photofrin-mediated pleural photodynamic therapy (pPDT). *Phys. Med. Biol.* **2017**, *63*, 015031. [[CrossRef](#)]
23. Patterson, M.S.; Wilson, B.C.; Graff, R. In vivo tests of the concept of photodynamic threshold dose in normal rat liver photosensitized by aluminum chlorosulphonated phthalocyanine. *Photochem. Photobiol.* **1990**, *51*, 343–349. [[CrossRef](#)] [[PubMed](#)]
24. Belashov, A.V.; Zhikhoreva, A.A.; Salova, A.V.; Belyaeva, T.N.; Litvinov, I.K.; Kornilova, E.S.; Semenova, I.V.; Vasyutinskii, O.S. Analysis of Radachlorin localization in living cells by fluorescence lifetime imaging microscopy. *J. Photochem. Photobiol. Biol.* **2023**, *243*, 112699. [[CrossRef](#)] [[PubMed](#)]
25. He, J.; Yang, L.; Yi, W.; Fan, W.; Wen, Y.; Miao, X.; Xiong, L. Combination of fluorescence-guided surgery with photodynamic therapy for the treatment of cancer. *Mol. Imaging* **2017**, *16*, 1536012117722911. [[CrossRef](#)]
26. Kustov, D.; Kozlikina, E.; Efendiev, K.; Loshchenov, M.; Grachev, P.; Maklygina, Y.S.; Trifonov, I.; Baranov, A.; Stranadko, E.; Panchenkov, D.; et al. Laser-induced fluorescent visualization and photodynamic therapy in surgical treatment of glial brain tumors. *Biomed. Opt. Express* **2021**, *12*, 1761–1773. [[CrossRef](#)]

27. Dysart, J.S.; Patterson, M.S. Photobleaching kinetics, photoproduct formation, and dose estimation during ALA induced PpIX PDT of MLL cells under well oxygenated and hypoxic conditions. *Photochem. Photobiol. Sci.* **2006**, *5*, 73–81. [[CrossRef](#)]
28. Sheng, C.; Jack Hoopes, P.; Hasan, T.; Pogue, B.W. Photobleaching-based dosimetry predicts deposited dose in ALA-PpIX PDT of rodent esophagus. *Photochem. Photobiol.* **2007**, *83*, 738–748. [[CrossRef](#)]
29. Dysart, J.S.; Patterson, M.S. Characterization of Photofrin photobleaching for singlet oxygen dose estimation during photodynamic therapy of MLL cells in vitro. *Phys. Med. Biol.* **2005**, *50*, 2597. [[CrossRef](#)]
30. Brancalion, L.; Magennis, S.W.; Samuel, I.D.; Namdas, E.; Lesar, A.; Moseley, H. Characterization of the photoproducts of protoporphyrin IX bound to human serum albumin and immunoglobulin G. *Biophys. Chem.* **2004**, *109*, 351–360. [[CrossRef](#)]
31. Kuimova, M.K.; Yahioglu, G.; Levitt, J.A.; Suhling, K. Molecular rotor measures viscosity of live cells via fluorescence lifetime imaging. *J. Am. Chem. Soc.* **2008**, *130*, 6672–6673. [[CrossRef](#)] [[PubMed](#)]
32. Aigner, D.; Dmitriev, R.I.; Borisov, S.; Papkovsky, D.B.; Klimant, I. pH-sensitive perylene bisimide probes for live cell fluorescence lifetime imaging. *J. Mater. Chem. B* **2014**, *2*, 6792–6801. [[CrossRef](#)] [[PubMed](#)]
33. Ogle, M.M.; Smith McWilliams, A.D.; Ware, M.J.; Curley, S.A.; Corr, S.J.; Martí, A.A. Sensing temperature in vitro and in cells using a BODIPY molecular probe. *J. Phys. Chem. B* **2019**, *123*, 7282–7289. [[CrossRef](#)] [[PubMed](#)]
34. Rahim, M.K.; Zhao, J.; Patel, H.V.; Lagouros, H.A.; Kota, R.; Fernandez, I.; Gratton, E.; Haun, J.B. Phasor Analysis of Fluorescence Lifetime Enables Quantitative Multiplexed Molecular Imaging of Three Probes. *Anal. Chem.* **2022**, *94*, 14185–14194. [[CrossRef](#)] [[PubMed](#)]
35. Stringari, C.; Cinquin, A.; Cinquin, O.; Digman, M.A.; Donovan, P.J.; Gratton, E. Phasor approach to fluorescence lifetime microscopy distinguishes different metabolic states of germ cells in a live tissue. *Proc. Natl. Acad. Sci. USA* **2011**, *108*, 13582–13587. [[CrossRef](#)]
36. Gorbunova, I.A.; Sasin, M.E.; Zhikhoreva, A.A.; Belashov, A.V.; Beltukova, D.M.; Semenova, I.V.; Vasyutinskii, O.S. Fluorescence Anisotropy in Radachlorin and Chlorin e6 in Water–Methanol Solutions under One- and Two-Photon Excitation. *Photonics* **2023**, *10*, 9. [[CrossRef](#)]
37. Lassalle, H.P.; Wagner, M.; Bezdetsnaya, L.; Guillemin, F.; Schneckenburger, H. Fluorescence imaging of Foscan<sup>®</sup> and Foslip in the plasma membrane and in whole cells. *J. Photochem. Photobiol. B Biol.* **2008**, *92*, 47–53. [[CrossRef](#)]
38. Yeh, S.C.A.; Diamond, K.R.; Patterson, M.S.; Nie, Z.; Hayward, J.E.; Fang, Q. Monitoring photosensitizer uptake using two photon fluorescence lifetime imaging microscopy. *Theranostics* **2012**, *2*, 817. [[CrossRef](#)]
39. Reichert, D.; Erkkilä, M.T.; Gesperger, J.; Wadiura, L.I.; Lang, A.; Roetzer, T.; Woehrer, A.; Andreeva, M.; Unterhuber, A.; Wilzbach, M.; et al. Fluorescence lifetime imaging and spectroscopic co-validation for protoporphyrin IX-guided tumor visualization in neurosurgery. *Front. Oncol.* **2021**, *11*, 741303. [[CrossRef](#)]
40. Mo, W.; Rohrbach, D.; Sunar, U. Imaging a photodynamic therapy photosensitizer in vivo with a time-gated fluorescence tomography system. *J. Biomed. Opt.* **2012**, *17*, 071306–071306. [[CrossRef](#)]
41. König, K.; Schneckenburger, H.; Rück, A.; Steiner, R. In vivo photoproduct formation during PDT with ALA-induced endogenous porphyrins. *J. Photochem. Photobiol. B Biol.* **1993**, *18*, 287–290. [[CrossRef](#)] [[PubMed](#)]
42. König, K.; Wabnitz, H.; Dietel, W. Variation in the fluorescence decay properties of haematoporphyrin derivative during its conversion to photoproducts. *J. Photochem. Photobiol. B Biol.* **1990**, *8*, 103–111. [[CrossRef](#)] [[PubMed](#)]
43. Kelbauskas, L.; Dietel, W. Internalization of Aggregated Photosensitizers by Tumor Cells: Subcellular Time-resolved Fluorescence Spectroscopy on Derivatives of Pyropheophorbide-a Ethers and Chlorin e6 under Femtosecond One- and Two-photon Excitation. *Photochem. Photobiol.* **2002**, *76*, 686–694. [[CrossRef](#)] [[PubMed](#)]
44. Belashov, A.V.; Zhikhoreva, A.A.; Gorbunova, I.A.; Sasin, M.E.; Shayakhmedov, S.S.; Semenova, I.V. Photophysical properties of Radachlorin photosensitizer in solutions of different pH, viscosity and polarity. *Spectrochim. Acta Part A Mol. Biomol. Spectrosc.* **2024**, *305*, 123480. [[CrossRef](#)]
45. Radapharma. Radachlorin Photosensitizer. Available online: <http://www.radapharma.ru/production/46-radachlorin-concentrate-for-production-of-intravenous-solution-035.html> (accessed on 27 August 2023).
46. Kochneva, E.V.; Filonenko, E.V.; Vakulovskaya, E.G.; Scherbakova, E.G.; Seliverstov, O.V.; Markichev, N.A.; Reshetnikov, A.V. Photosensitizer Radachlorin: Skin cancer (PDT) phase II clinical trials. *Photodiagn. Photodyn. Ther.* **2010**, *7*, 258–267. [[CrossRef](#)] [[PubMed](#)]
47. Privalov, V.A.; Lappa, A.V.; Kochneva, E.V. Five Years' Experience of Photodynamic Therapy with New Chlorin Photosensitizer. *Proc. Spie* **2005**, *5863*, 586310.
48. Filonenko, E.V.; Sokolov, V.V.; Chissov, V.I.; Lukyanets, E.A.; Vorozhtsov, G.N. Photodynamic therapy of early esophageal cancer. *Photodiagn. Photodyn. Ther.* **2008**, *5*, 187–190. [[CrossRef](#)]
49. Shafirstein, G.; Battoo, A.; Harris, K.; Baumann, H.; Gollnick, S.O.; Lindenmann, J.; Nwogu, C.E. Photodynamic Therapy of Non-Small Cell Lung Cancer. Narrative Review and Future Directions. *Ann. Am. Thorac. Soc.* **2016**, *13*, 265–275. [[CrossRef](#)]
50. Shiryaev, A.A.; Musaev, G.K.; Levkin, V.V.; Reshetov, I.V.; Loshchenov, M.V.; Alekseeva, P.M.; Volkov, V.V.; Linkov, K.G.; Makarov, V.I.; Shchekoturov, I.O.; et al. Combined treatment of nonresectable cholangiocarcinoma complicated by obstructive jaundice. *Photodiagn. Photodyn. Ther.* **2019**, *26*, 218–223. [[CrossRef](#)]
51. Seo, C.W.; Kim, Y.K.; An, J.L.; Kim, J.S.; Kwon, P.S.; Yu, Y.B. The effect of photodynamic therapy using Radachlorin on biofilm-forming multidrug-resistant bacteria. *Osong Public Health Res. Perspect.* **2022**, *13*, 290–297. [[CrossRef](#)]

52. Svyatchenko, V.A.; Nikonov, S.D.; Mayorov, A.P.; Gelfond, M.L.; Loktev, V.B. Antiviral photodynamic therapy: Inactivation and inhibition of SARS-CoV-2 in vitro using methylene blue and Radachlorin. *Photodiagn. Photodyn. Ther.* **2021**, *33*, 102112. [[CrossRef](#)] [[PubMed](#)]
53. Belashov, A.V.; Zhikhoreva, A.A.; Belyaeva, T.N.; Salova, A.V.; Kornilova, E.S.; Semenova, I.V.; Vasyutinskii, O.S. Machine learning assisted classification of cell lines and cell states on quantitative phase images. *Cells* **2021**, *10*, 2587. [[CrossRef](#)] [[PubMed](#)]
54. Zhikhoreva, A.A.; Belashov, A.V.; Belyaeva, T.N.; Salova, A.V.; Litvinov, I.K.; Kornilova, E.S.; Semenova, I.V.; Vasyutinskii, O.S. Comparative analysis of Radachlorin accumulation, localization, and photobleaching in three cell lines by means of holographic and fluorescence microscopy. *Photodiagn. Photodyn. Ther.* **2022**, *39*, 102973. [[CrossRef](#)]
55. Wyld, L.; Smith, O.; Lawry, J.; Reed, M.; Brown, N. Cell cycle phase influences tumour cell sensitivity to aminolaevulinic acid-induced photodynamic therapy in vitro. *Br. J. Cancer* **1998**, *78*, 50–55. [[CrossRef](#)] [[PubMed](#)]
56. Sano, M.; Furuta, T.; Takahira, K.; Kajimura, M.; Hanai, H.; Kohno, E.; Hirano, T.; Hishida, A. Cell-cycle-dependent efficacy of photodynamic therapy with ATX-S10 (Na). *Lasers Med. Sci.* **2005**, *20*, 1–5. [[CrossRef](#)]
57. Belashov, A.; Zhikhoreva, A.; Belyaeva, T.; Kornilova, E.; Salova, A.; Semenova, I.; Vasyutinskii, O. In vitro monitoring of photoinduced necrosis in HeLa cells using digital holographic microscopy and machine learning. *JOSA A* **2020**, *37*, 346–352. [[CrossRef](#)]
58. Awasthi, K.; Yamamoto, K.; Furuya, K.; Nakabayashi, T.; Li, L.; Ohta, N. Fluorescence Characteristics and Lifetime Images of Photosensitizers of Talaporfin Sodium and Sodium Pheophorbide a in Normal and Cancer Cells. *Sensors* **2015**, *15*, 11417–11430. [[CrossRef](#)]
59. Helmerich, D.A.; Beliu, G.; Matikonda, S.S.; Schnermann, M.J.; Sauer, M. Photoblueing of organic dyes can cause artifacts in super-resolution microscopy. *Nat. Methods* **2021**, *18*, 253–257. [[CrossRef](#)]
60. Liu, X.; Lin, D.; Becker, W.; Niu, J.; Yu, B.; Liu, L.; Qu, J. Fast fluorescence lifetime imaging techniques: A review on challenge and development. *J. Innov. Opt. Health Sci.* **2019**, *12*, 1930003. [[CrossRef](#)]
61. Bopp, M.A.; Jia, Y.; Li, L.; Cogdell, R.J.; Hochstrasser, R.M. Fluorescence and photobleaching dynamics of single light-harvesting complexes. *Proc. Natl. Acad. Sci. USA* **1997**, *94*, 10630–10635. [[CrossRef](#)]
62. Becker, W. Fluorescence lifetime imaging—techniques and applications. *J. Microsc.* **2012**, *247*, 119–136. [[CrossRef](#)] [[PubMed](#)]
63. Ferulova, I.; Lihachev, A.; Spigulis, J. Photobleaching effects on in vivo skin autofluorescence lifetime. *J. Biomed. Opt.* **2015**, *20*, 051031. [[CrossRef](#)] [[PubMed](#)]
64. Dysart, J.S.; Singh, G.; Patterson, M.S. Calculation of Singlet Oxygen Dose from Photosensitizer Fluorescence and Photobleaching during mTHPC Photodynamic Therapy of MLL Cells. *Photochem. Photobiol.* **2005**, *81*, 196–205. [[CrossRef](#)] [[PubMed](#)]
65. James, N.S.; Cheruku, R.R.; Missert, J.R.; Sunar, U.; Pandey, R.K. Measurement of cyanine dye photobleaching in photosensitizer cyanine dye conjugates could help in optimizing light dosimetry for improved photodynamic therapy of cancer. *Molecules* **2018**, *23*, 1842. [[CrossRef](#)] [[PubMed](#)]
66. Ascencio, M.; Collinet, P.; Farine, M.; Mordon, S. Protoporphyrin IX fluorescence photobleaching is a useful tool to predict the response of rat ovarian cancer following hexaminolevulinic acid photodynamic therapy. *Lasers Surg. Med. Off. J. Am. Soc. Laser Med. Surg.* **2008**, *40*, 332–341. [[CrossRef](#)] [[PubMed](#)]

**Disclaimer/Publisher’s Note:** The statements, opinions and data contained in all publications are solely those of the individual author(s) and contributor(s) and not of MDPI and/or the editor(s). MDPI and/or the editor(s) disclaim responsibility for any injury to people or property resulting from any ideas, methods, instructions or products referred to in the content.